



OPEN

Bionic adaptive fault-tolerant control of non-Gaussian stochastic attitude hypersonic vehicle

Kai-Yu Hu[✉], Kun Zhu & Wenjing Sun

This study investigates an adaptive fault-tolerant control (FTC) for hypersonic flight vehicles (HFVs) with incipient faults and non-Gaussian stochastic output attitudes. In the nonlinear HFV dynamics, a hybrid fuzzy approximation method achieves the linearization, then the stochastic outputs are transformed into probability density functions (PDFs) via rational square root B-spline. The disturbance and faults are estimated simultaneously by an adaptive augmented observer. Then actuator faults are compensated by a bionic adaptive fault-tolerant controller to ensure that the output PDFs accurately track the expected PDFs, thereby matching actual attitude angles with the desired ones, the bionic prey adaptive law can make FTC accurately repair the incipient fault deviations. Lyapunov theory proves the robust stability of the scheme, and simulation illustrates the effectiveness.

In recent years, some new advances in modelling, fault estimation and fault-tolerant control (FTC) for hypersonic flight vehicle (HFV) or other kinds of spacecrafts have been achieved^{1–5}. Where the study of uncertainties can improve the algorithm reliability, which mainly focus on the uncertainty of parameters, actuator faults and environment. In^{6,7}, the disturbance observer (DOB) was investigated to deal with the HFV system with disturbance or uncertain wind effects. Various subsystems of HFV have a variety of fault types^{8–10}. In¹¹, an estimation algorithm was proposed to estimate the time-varying bias and gain faults. In¹², a fault tolerant strategy was designed for the re-entry HFV with mixed aerodynamic surfaces under uncertainties and faults. In^{13,14}, a novel adaptive FTC was proposed for HFV with input constraints and uncertain parameters. This paper simultaneously studies the FTC method for the approximated nonlinear HFV with attitude output uncertainties and actuator faults.

Laser weapons can counter HFV but require time to accumulate energy to burn obstacles^{15,16}. Hence, one anti-laser method is attitude active randomization. Output uncertainty should also be investigated because of the harsh environment. Given these uncertain outputs, FTC for non-Gaussian stochastic systems can improve the HFV reliability, and linear B-spline interpolation is a method to obtain stochastic distributions¹⁷. Other complex interpolations meet the high reliability are also useful. For example in¹⁸, the rational square root algorithm was presented for the non-Gaussian output probability density function (PDF).

New progress is achieved in the reconstruction and tracking control of systems with singularity, time-delay functions and non-Gaussian stochastic outputs. Complex fuzzy approximation theory is an effective tool for solving complex nonlinear problems^{19,20}. In²¹, T–S fuzzy theory was used for non-Gaussian stochastic systems, whilst a sliding-mode algorithm compensated for the fault impacts. In²², the measurable premise variables and estimations of the immeasurable premise variables were used for fuzzy controllers. In^{23,24}, the state feedback robust controller and output feedback dynamic control strategy were designed for complex singular systems. In²⁵, algorithms were proposed for the singular time-delay systems with non-Gaussian stochastic output and PDF approximation error. The time delay problem was investigated in^{26,27}, in which the adaptive-robust delay controllers were used to solve the problem of the Euler–Lagrange systems. An adaptive observer and fault-tolerant PI controller were designed because of the singular and delay of non-Gaussian systems²⁸. In²⁹, the enhanced robust observer and neurocontrollers were presented for the systems with output uncertainties to repair faults and shield disturbance. The main considerations in this paper include fuzzy linearization, singularity, exogenous interference and non-Gaussian stochastic FTC.

We use PDF as the algorithm variable to enable the controller to receive accurate internal information of the attitude angles, then the output PDF shape can perfectly match the expected value when the fault occurs, finally the FTC of HFV with non-Gaussian stochastic attitudes is realized. The contributions and innovations of this study are as follows:

Aviation Technology Research Institute, China Aerospace Science and Industry Corporation, Beijing 100143, China.
✉email: hkywuyue@163.com

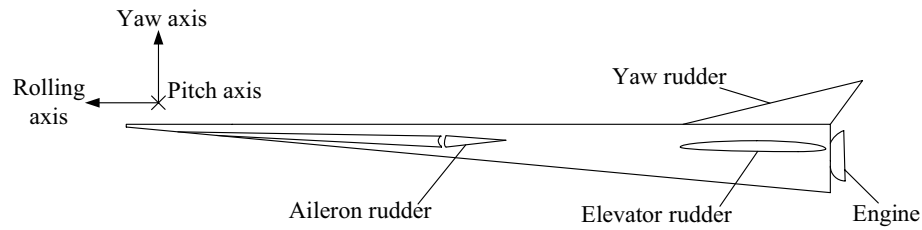


Figure 1. Simplified structure of HFV.

1. Proposing a non-Gaussian stochastic HFV system to solve the problem of stochastic attitude angle modeling and real-time statistics of the distribution information. Displaying the fault information using PDF deformations is more accurate than the conventional attitude angle signals.
2. Proposing a multi-fuzzy approximation scheme to linearize the HFV and disturbance interconnect systems, then designing an adaptive DOB and proving the robust stability.
3. Designing an improved adaptive fuzzy fault estimation and FTC scheme by mimicking animal predation behavior, which are better than the traditional method when diagnosing and compensating for incipient faults.

Section 2 introduces the HFV model with non-Gaussian stochastic attitude angles. Section 3.1 presents an augmented estimation observer to estimate the incipient deviation fault and disturbance. Section 3.2 proposes a improved adaptive compensation controller. Section 3.3 designs the bionic prey adaptive law. Lastly, Sect. 4 verifies the methods.

System and fault models

The rudders of HFV are shown in Fig. 1. The stochastic attitudes are generated by the deterministic rudder commands combining with uncertain environment or stochastic jet rudders. Fixed rudders can achieve stochastic attitude tracking control.

With reference to¹⁴, the following reentry HFV model with non-Gaussian stochastic attitude angles is designed:

$$\begin{aligned}
 E\dot{x}(t) &= A(x(t))x(t) + A_d(x(t - \tau(t)))x(t - \tau(t)) \\
 &\quad + B(x(t))u(t) + NF_{com}(t) + B_d d(t) \\
 x(t) &= \phi(t), t \in [-t, 0] \\
 V(t) &= D(\Xi x(t)) \\
 \gamma(\rho, u(t)) &= \Phi^2(C(\rho)V(t))^2
 \end{aligned}
 \tag{1}$$

where $x(t) = [\bar{p}(t) \ \bar{q}(t) \ \bar{r}(t)]^T$ and $\bar{p}(t)$, $\bar{q}(t)$ and $\bar{r}(t)$ are the pitch, roll and yaw rates, respectively; $\rho = [\rho_1 \ \rho_2 \ \rho_3]^T$ and ρ_1, ρ_2 and ρ_3 are the bank, sideslip, attack angles, respectively; $u(t) = [\delta_e \ \delta_a \ \delta_r]^T$ is the control surface deflection and δ_e, δ_a and δ_r are the elevator, aileron and yaw rudder deflections, respectively; $V(t) \in R^3$ is the weight vector and $\tau(t)$ is the time-varying delay function that satisfies $0 \leq \tau(t) \leq t$; $\phi(t)$ is an initial rudder rate function and $F_{com}(t) \in R^3$ is the rudder fault vector and set $F_{com}(t)$ as follows:

$$F_{com}(t) \subseteq \{F_1(t), F(t)\} \tag{2}$$

$F_1(t)$ is the incipient rudder deviation satisfying (3) with reference to³⁰. $F(t)$ is the standard deviation fault, which does not meet (3).

$$\|F_1(t)/u(t)\| \leq 10\% \tag{3}$$

The incipient deviation is characterised with three features³⁰: (1) from the qualitative aspect, the deteriorated degree is insufficient to trigger any pre-set fault alarms; (2) from the quantitative aspect, the deviation percent ranks from 1 to 10%, these slight abnormalities are easily affected by the systems; (3) it will develop into a catastrophic fault or the fault like $F(t)$.

$A(x(t))$ and $B(x(t)) \in R^{3 \times 3}$ are the nonlinear matrix functions that satisfy the following equations:

$$A(x(t)) = J^{-1}\Theta(x(t))J \tag{4}$$

$$B(x(t)) = J^{-1}G \tag{5}$$

where $J \in R^{3 \times 3}$ is the inertia matrix, G is the control allocation matrix distributes the control torque to the control surfaces:

$$\Theta(x(t)) = \begin{bmatrix} 0 & \bar{r}(t) & -\bar{q}(t) \\ -\bar{r}(t) & 0 & \bar{p}(t) \\ \bar{q}(t) & -\bar{p}(t) & 0 \end{bmatrix}, \quad G = \begin{bmatrix} g_{p,\delta_e} & g_{p,\delta_a} & g_{p,\delta_r} \\ g_{q,\delta_e} & g_{q,\delta_a} & g_{q,\delta_r} \\ g_{r,\delta_e} & g_{r,\delta_a} & g_{r,\delta_r} \end{bmatrix}.$$

$E, B_\phi, N \in R^{3 \times 3}$ are the parameter matrices, where $rank(E) = q < 3$. $D(\cdot) \in R^{3 \times 3}$ is a transformation matrix function contains an equivalent integral and a linear transformation functions. $\Xi x(t) = [\dot{\rho}_1 \ \dot{\rho}_2 \ \dot{\rho}_3]^T$ represents the angular rates and Ξ satisfies (6).

$$\Xi = \begin{bmatrix} \cos \rho_3 & 0 & \sin \rho_3 \\ \sin \rho_3 & 0 & -\cos \rho_3 \\ 0 & 1 & 0 \end{bmatrix} \tag{6}$$

Output (7) describes the non-Gaussian stochastic attitude angles, whilst its PDFs are approximated by the rational square root B-spline functions. The re-entry HFV model has three outputs. Thus,

$$\begin{aligned} \gamma(\rho, u(t)) &= [\gamma_1(\rho_1, u(t)) \ \gamma_2(\rho_2, u(t)) \ \gamma_3(\rho_3, u(t))]^T \\ &= [\Phi^2(C_{\rho_1} V(t))^2 \ \Phi^2(C_{\rho_2} V(t))^2 \ \Phi^2(C_{\rho_3} V(t))^2]^T \end{aligned} \tag{7}$$

where

$$\begin{aligned} C(\rho) &= \begin{bmatrix} C_{\rho_1} \\ C_{\rho_2} \\ C_{\rho_3} \end{bmatrix} = \begin{bmatrix} \varphi_{11}(\rho_1) & \dots & \varphi_{13}(\rho_1) \\ \varphi_{21}(\rho_2) & \dots & \varphi_{23}(\rho_2) \\ \varphi_{31}(\rho_3) & \dots & \varphi_{33}(\rho_3) \end{bmatrix}, \\ V &= [w_1, \dots, w_3]^T, \\ \Phi &= 1/\sqrt{V^T(t)\Sigma_1 V(t)}, \\ \Sigma_1 &= \int_a^b C^T(\rho)C(\rho)d\rho. \end{aligned}$$

And $\varphi_{\tilde{i}\tilde{j}}(\rho)$ ($i = 1, 2, 3, \tilde{i} = 1, 2, 3$) are the predetermined basis functions; w_i are the tracking weights; γ_1, γ_2 and γ_3 are the PDFs of the bank, sideslip and attack angles, respectively. Compared with the traditional models, (1) describes the microscopic stochastic details of the output attitude angles. The PDF deformation can display additional information that the classic outputs cannot show using mean and variance, thereby improving control accuracy.

Remark 1 The mean of the non-Gaussian attitude angles reveals the overall performance and is an important reference for the HFV full-process tracking control and task execution. Our model can calculate and control the mean in real time using (8). Arithmetic * is the matrix Hadamard product.

$$\mu_{mean} = \int_a^b \rho * \gamma(\rho, u(t))d\rho \tag{8}$$

The nonlinear external disturbance is expressed as follows:

$$\begin{cases} \dot{\omega}(t) = \Omega(t)\omega(t) \\ d(t) = T(t)\omega(t) \end{cases} \tag{9}$$

where $\omega(t), d(t) \in R^{3 \times 1}, T(t), \Omega(t) \in R^{3 \times 3}, \Omega(t)$ is the functions describe the distance between disturbance source and HFV.

Systems (1) is linearised using double fuzzy approximation. The i th rule: IF $\varpi_1(t)$ is β_{i1} , and ..., and $\varpi_\sigma(t)$ is $\beta_{i\sigma}$, THEN:

$$\begin{aligned} E_i \dot{x}(t) &= A_i x(t) + A_{id} x(t - \tau(t)) + B_i u(t) + N_i F_{com}(t) + B_{id} d(t) \\ V(t) &= D_i \Xi_i x(t) \\ x(t) &= \phi(t), \quad t \in [-\iota, 0] \\ \gamma(\rho, u(t)) &= \Phi^2(C(\rho)V(t))^2 \end{aligned} \tag{10}$$

The w th rule: IF $\Delta_1(t)$ is β_{w1} , and..., and $\Delta_v(t)$ is β_{wv} , THEN :

$$\begin{cases} \dot{\omega}(t) = \Omega_w \omega(t) \\ d(t) = T_w \omega(t) \end{cases} \tag{11}$$

where in (10), $\varpi_j (j = 1, \dots, \sigma)$ are the prerequisite variables and $\beta_{ij} (i = 1, \dots, \bar{n})$ are the fuzzy sets; in (11), $\Delta_\vartheta (\vartheta = 1, \dots, v)$ are the prerequisite variables and $\beta_{w\vartheta} (w = 1, \dots, \bar{m})$ are the fuzzy sets.

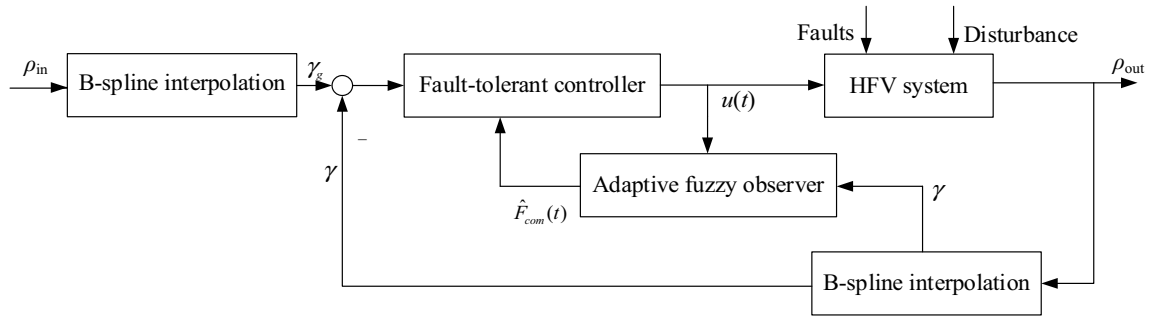


Figure 2. Block diagram of fault-tolerant control.

$$\begin{cases} h_i(\varpi(t)) = \prod_{j=1}^{\sigma} \beta_{ij}(\varpi(t)) / \sum_{i=1}^{\bar{n}} \prod_{j=1}^{\sigma} \beta_{ij}(\varpi(t)) \geq 0 \\ h_w(\Delta(t)) = \prod_{\vartheta=1}^{\nu} \beta_{w\vartheta}(\Delta(t)) / \sum_{w=1}^{\bar{m}} \prod_{\vartheta=1}^{\nu} \beta_{w\vartheta}(\Delta(t)) \geq 0 \\ \sum_{i=1}^{\bar{n}} h_i(\varpi(t)) = \sum_{w=1}^{\bar{m}} h_w(\Delta(t)) = 1 \end{cases} \quad (12)$$

Figure 2 shows the overall block diagram of the HFV system fault-tolerant scheme.

Assumption 1 $\|F_1(t)\|, \|F(t)\| \leq M_f, \|d(t)\| \leq M_d$. M_f and M_d are two positive scalars.

Assumption 2 There exist two reversible matrices L_1 and L_2 such that: $L_{i1}A_{id}L_{i2} = [A_{id1} \ 0; 0 \ A_{id2}]$, $L_{i1}E_iL_{i2} = [I_q \ 0; 0 \ 0]$, $L_{i1}A_iL_{i2} = [A_{i1} \ 0; 0 \ I_{3-q}]$.

Remark 2 The disturbance source cannot have infinite power, so the amplitude of the electromagnetic wave transmitted by it is bounded. Therefore, setting bounded external disturbance can better reflect the real war scene. The rudders of HFV have a software and hardware dual limiting scheme. Even if there is a very small probability that breaks the two limits, the aerodynamic effect of the deflection angle beyond 180 deg is the same as the effect of the remaining angle after subtracting 180 deg. Therefore, it is reasonable to set the rudder fault to be bounded. In engineering, the decoupled HFV system reflects a flight environment with directional disturbance, it slows down the response speed of some control channels, while the control channels facing away from the disturbance source or away from the interference direction still maintain fast response. Hence the undisturbed channel is decoupled from the other channels. For example, the roll rudders is another set of independent execution system, if it is undisturbed, it is decoupled obviously. Therefore, it is reasonable to set up a singular HFV system that can be uncoupled.

Given the singularity and Assumption 2, systems (10) and (11) can be transformed as follows:

$$\begin{aligned} \dot{x}_1(t) &= \sum_{i=1}^{\bar{n}} \sum_{w=1}^{\bar{m}} h_i(\varpi(t))h_w(\Delta(t))[A_{i1}x_1(t) + A_{id1}x_1(t - \tau(t)) \\ &\quad + B_{i1}u(t) + N_{i1}F_{com}(t) + B_{id1}T_w\omega(t)] \\ x_2(t) &= \sum_{i=1}^{\bar{n}} \sum_{w=1}^{\bar{m}} h_i(\varpi(t))h_w(\Delta(t))[-A_{id2}x_2(t - \tau(t)) - B_{i2}u(t) \\ &\quad - N_{i2}F_{com}(t) - B_{id2}T_w\omega(t)] \\ V(t) &= \sum_{i=1}^{\bar{n}} \sum_{w=1}^{\bar{m}} h_i(\varpi(t))h_w(\Delta(t))(D_{i1}\Xi_{i1}x_1(t) + D_{i2}\Xi_{i2}x_2(t)) \\ \dot{\omega}(t) &= \sum_{i=1}^{\bar{n}} \sum_{w=1}^{\bar{m}} h_i(\varpi(t))h_w(\Delta(t))\Omega_w\omega(t) \end{aligned} \quad (13)$$

where $B_{i1}, B_{id1}, N_{i1} \in R^{q \times 3}$, $B_{i2}, B_{id2}, N_{i2} \in R^{(3-q) \times 3}$, $D_{i1}\Xi_{i1} \in R^{3 \times q}$, $D_{i2}\Xi_{i2} \in R^{3 \times (3-q)}$, which satisfies: $L_{i2}B_i = [B_{i1}; B_{i2}]$, $L_{i2}B_{id} = [B_{id1}; B_{id2}]$, $D_i\Xi_iL_{i1} = [D_{i1}\Xi_{i1} \ D_{i2}\Xi_{i2}]$, $L_{i2}N_i = [N_{i1}; N_{i2}]$.

This study is dedicated to providing the fault-tolerant control scheme for the faults with different deviation amplitudes in the HFV with stochastic attitude angles. The following sections are the scheme design process.

Fault compensation control scheme

Fault estimation. Disturbance and singularity lead to system uncertainty and inconsistent response. Disturbance can contaminate useful signals to severely distort system information, and the observer cannot accurately estimate faults, which can lead to instability. Singularity is an inherent property. Neglecting singularity can lead to poor tracking performance of the control scheme and difficult to be widely applied at the engineering site.

To solve these problems, two state error functions of fast-slow subsystems and one disturbance error function are constructed. By substituting these three functions into the performance indicators, new methods ensure that the system is H^∞ stable.

Definition 1 To simplify the expression, we set the double fuzzy approximation superposition function shown in system (13) to satisfy:

$$\Lambda_{(i,w)}(\varpi, \Delta) = \sum_{i=1}^{\bar{n}} \sum_{w=1}^{\bar{m}} h_i(\varpi(t))h_w(\Delta(t)) \tag{14}$$

If there is only one type of linear weight mode in a double fuzzy approximation process, (14) will degenerate into a single fuzzy approximation superposition function, that is, satisfies:

$$\Lambda_{(i,w)}(\varpi, \Delta) = \sum_{i=1}^{\bar{n}} h_i(\varpi(t)) \text{ or } \sum_{w=1}^{\bar{m}} h_w(\Delta(t)) \tag{15}$$

This definition enables the simplification and unification of symbols in the derivation process.

The following system is obtained by combining systems (1) and (9) and letting $\zeta(t) = [x_1^T(t) \ \omega^T(t)]^T$:

$$\begin{aligned} \dot{\zeta}(t) &= \Lambda_{(i,w)}(\varpi, \Delta)[A_{iw0}\zeta(t) + A_{id0}\zeta(t - \tau(t)) + B_{i0}u(t) + N_{i0}F_{com}(t)] \\ x_2 &= \Lambda_{(i,w)}(\varpi, \Delta)[-A_{id2}x_2(t - \tau(t)) - B_{i2}u(t) - N_{i2}F_{com}(t) - B_{id2}T_w\omega(t)] \\ V(t) &= \Lambda_{(i,w)}(\varpi, \Delta)(D_{i1}\Xi_{i1}x_1(t) + D_{i2}\Xi_{i2}x_2(t)) \\ &= \Lambda_{(i,w)}(\varpi, \Delta)(D_{i0}\Xi_{i0}\zeta(t) + D_{i2}\Xi_{i2}x_2(t)) \end{aligned} \tag{16}$$

where $A_{iw0} = [A_{i1} \ B_{id1} \ T_w; 0 \ \Omega_w]$, $A_{id0} = [A_{id1} \ 0; 0 \ 0]$, $B_{i0} = [B_{i1}; 0]$, $N_{i0} = [N_{i1}; 0]$ and $D_{i0}\Xi_{i0} = [D_{i1}\Xi_{i1} \ 0]$. The full-order DOB is designed as follows:

$$\begin{aligned} \dot{\hat{\zeta}}(t) &= \Lambda_{(i,w)}(\varpi, \Delta)[A_{iw0}\hat{\zeta}(t) + A_{id0}\hat{\zeta}(t - \tau(t)) + B_{i0}u(t) + K_{i1}\varepsilon(t)] \\ \hat{x}_2 &= \Lambda_{(i,w)}(\varpi, \Delta)[-A_{id2}\hat{x}_2(t - \tau(t)) - B_{i2}u(t) - N_{i2}F_{com}(t) - B_{id2}T_w\hat{\omega}(t)] \\ \hat{V}(t) &= \Lambda_{(i,w)}(\varpi, \Delta)(D_{i0}\Xi_{i0}\hat{\zeta}(t) + D_{i2}\Xi_{i2}\hat{x}_2(t)) \\ \varepsilon(t) &= \int_a^b (\sqrt{\gamma} - \sqrt{\hat{\gamma}})d\rho \end{aligned} \tag{17}$$

The derivation process of $\varepsilon(t)$ is expressed as follows:

$$IF \left\{ \begin{array}{l} \varpi_1(t) \text{ is } \beta_{i1}, \text{ and } \dots \text{ and } \varpi_\sigma(t) \text{ is } \beta_{i\sigma} \\ \Delta_1(t) \text{ is } \beta_{w1}, \text{ and } \dots \text{ and } \Delta_\nu(t) \text{ is } \beta_{w\nu} \end{array} \right., \text{ THEN :}$$

$$\begin{aligned} \varepsilon(t) &= \Sigma_2[\hat{\Phi}(D_{i0}\Xi_{i0}\zeta(t) + D_{i2}\Xi_{i2}x_2(t)) - \hat{\Phi}(D_{i0}\Xi_{i0}\hat{\zeta}(t) + D_{i2}\Xi_{i2}\hat{x}_2(t))] \\ &\quad + \hat{\Phi}(D_{i0}\Xi_{i0}\zeta(t) + D_{i2}\Xi_{i2}x_2(t)) - \hat{\Phi}(D_{i0}\Xi_{i0}\hat{\zeta}(t) + D_{i2}\Xi_{i2}\hat{x}_2(t))] \\ &= \hat{\Phi}\Sigma_2(D_{i0}\Xi_{i0}e_\zeta(t) + D_{i2}\Xi_{i2}e_2(t)) + \hat{\Phi}\Sigma_2(D_{i0}\Xi_{i0}\zeta(t) \\ &\quad + D_{i2}\Xi_{i2}x_2(t))(\Phi/\hat{\Phi} - 1) \end{aligned} \tag{18}$$

On the basis of (19), error function (18) is derived as (20):

$$1/\hat{\Phi} - 1/\Phi = \lambda_1(\|\hat{V}(t)\| - \|V^T(t)\|) \tag{19}$$

$$\begin{aligned} \varepsilon(t) &= \Lambda_{(i,w)}(\varpi, \Delta)[\hat{\Phi}\Sigma_2(D_{i0}\Xi_{i0}e_\zeta(t) + D_{i2}\Xi_{i2}e_2(t)) \\ &\quad + \hat{\Phi}\Sigma_2(D_{i0}\Xi_{i0}\zeta(t) + D_{i2}\Xi_{i2}x_2(t))\Phi\lambda_1(\|\hat{V}(t)\| - \|V^T(t)\|)] \end{aligned} \tag{20}$$

By combining (16) and (17), the full-order observer error system is established as follows:

$$\begin{aligned} \dot{e}_\zeta(t) &= \dot{\zeta} - \dot{\hat{\zeta}} \\ &= \Lambda_{(i,w)}(\varpi, \Delta) \{ [A_{iw0}e_\zeta(t) + A_{id0}e_\zeta(t - \tau(t)) + N_{i0}F_{com}(t) \\ &\quad - L_{i3}\Sigma_2 D_{i0}\Xi_{i0}e_\zeta - L_{i3}\Sigma_2 D_{i2}\Xi_{i2}e_2] + L_{i3}\Sigma_2 V\Phi\lambda_1(\|V\| - \|\hat{V}\|) \} \end{aligned} \tag{21}$$

where $L_{i3} = \hat{\Phi}K_{i1}$ and $\Sigma_2 = \int_a^b C(\rho)d\rho$.

In the estimation process, the observer is constructed to eliminate the disturbance and estimate the faults as follows:

$$\begin{aligned} \hat{x}_1(t) &= \Lambda_{(i,w)}(\varpi, \Delta) [A_{i1}\hat{x}_1(t) + A_{id1}\hat{x}_1(t - \tau(t)) \\ &\quad + B_{i1}u(t) + N_{i1}\hat{F}_{com}(t) + B_{id1}T_w\hat{\omega}(t) + K_{i2}\varepsilon(t)] \\ \hat{x}_2(t) &= \Lambda_{(i,w)}(\varpi, \Delta) [-A_{id2}\hat{x}_2(t - \tau(t)) - B_{i2}u(t) - N_{i2}\hat{F}_{com}(t) - B_{id2}T_w\hat{\omega}(t)] \\ \hat{V}(t) &= \Lambda_{(i,w)}(\varpi, \Delta) (D_{i1}\Xi_{i1}\hat{x}_1(t) + D_{i2}\Xi_{i2}\hat{x}_2(t)) \\ \hat{\gamma}(\rho, u(t)) &= \hat{\Phi}^2(C(\rho)\hat{V}(t))^2 \\ \hat{F}_{com}(t) &= \Lambda_{(i,w)}(\varpi, \Delta) (-prey\{\Gamma_{i1}\}\hat{F}_{com}(t) + prey\{\Gamma_{i2}\}\varepsilon(t)) \end{aligned} \tag{22}$$

where $prey\{\cdot\}$ means the prey adaptive strategy designed for different fault amplitudes and does not affect the derivation. The estimation error dynamics can be expressed as (24) by setting (23):

$$\begin{cases} \tilde{F}_{com}(t) = F_{com}(t) - \hat{F}_{com}(t) \\ e_1 = x_1 - \hat{x}_1 \end{cases} \tag{23}$$

$$\begin{aligned} \dot{e}_1(t) &= \Lambda_{(i,w)}(\varpi, \Delta) [A_{i1}e_1(t) + A_{id1}e_1(t - \tau(t)) + N_{i1}\tilde{F}_{com}(t) + B_{id1}T_w\tilde{\omega}(t) \\ &\quad - L_{i4}\Sigma_2 D_{i1}\Xi_{i1}e_1 - L_{i4}\Sigma_2 D_{i2}\Xi_{i2}e_2 + L_{i4}\Sigma_2 V\Phi\lambda_1(\|V\| - \|\hat{V}\|)] \end{aligned} \tag{24}$$

where $L_{i4} = \hat{\Phi}K_{i2}$. Thence the fault estimation dynamic is as follows:

$$\begin{aligned} \dot{\hat{F}}_{com}(t) &= \Lambda_{(i,w)}(\varpi, \Delta) [-prey\{\Gamma_{i1}\}\hat{F}_{com}(t) + L_{i5}\Sigma_2 D_{i1}\Xi_{i1}e_1 \\ &\quad + L_{i5}\Sigma_2 D_{i2}\Xi_{i2}e_2 - L_{i5}\Sigma_2 V\Phi\lambda_1(\|V\| - \|\hat{V}\|)] \end{aligned} \tag{25}$$

and $L_{i5} = \hat{\Phi}prey\{\Gamma_{i2}\}$. The following equation can be derived by combining systems (21), (24) and (25):

$$\begin{aligned} \begin{bmatrix} \dot{e}_\zeta(t) \\ \dot{e}_1(t) \\ \dot{\hat{F}}_{com}(t) \end{bmatrix} &= \Lambda_{(i,w)}(\varpi, \Delta) \left[\bar{A}_{iw} \begin{bmatrix} e_\zeta(t) \\ e_1(t) \\ \hat{F}_{com}(t) \end{bmatrix} + \begin{bmatrix} A_{id0}e_\zeta(t - \tau(t)) \\ A_{id1}e_1(t - \tau(t)) \\ 0 \end{bmatrix} \right] \\ &\quad + \begin{bmatrix} N_{i0}F_{com}(t) \\ N_{i1}F_{com}(t) \\ 0 \end{bmatrix} + \begin{bmatrix} -L_{i3}\Sigma_2 D_{i2}\Xi_{i2}e_2 \\ -L_{i4}\Sigma_2 D_{i2}\Xi_{i2}e_2 \\ L_{i5}\Sigma_2 D_{i2}\Xi_{i2}e_2 \end{bmatrix} + \begin{bmatrix} L_{i3}\Sigma_2 h_1 \\ L_{i4}\Sigma_2 h_2 \\ -L_{i5}\Sigma_2 h_2 \end{bmatrix} \end{aligned} \tag{26}$$

where

$$\begin{aligned} \bar{A}_{iw} &= \begin{bmatrix} A_{iw0} - L_{i3}\Sigma_2 D_{i0}\Xi_{i0} & 0 & 0 \\ \bar{T}_{iw} & A_{i1} - L_{i4}\Sigma_2 D_{i1}\Xi_{i1} & -N_{i1} \\ 0 & L_{i5}\Sigma_2 D_{i1}\Xi_{i1} & -\Gamma_{i1} \end{bmatrix}, \\ \bar{T}_{iw} &= [0 \ B_{id1}T_w], \\ h_1 &= V\Phi\lambda_1(\|V\| - \|\hat{V}\|), \\ h_2 &= V\Phi\lambda_2(\|V\| - \|\hat{V}\|) \end{aligned}$$

The reference output s_∞ is defined as follows:

$$s_\infty = C_1 e_\zeta(t) + C_2 e_1(t) + C_3 e_1(t - \tau(t)) + C_4 \tilde{F}_{com}(t) + C_5 e_2(t) \tag{27}$$

For $\mu_1 > 0$ and $\mu_2 > 0$, the robust performance indicator is defined as follows:

$$J_\infty = \|s_\infty\|^2 - \mu_1^2 \|F_{com}(t)\|^2 - \mu_2^2 \|e_2(t)\|^2 - \bar{\delta}(Q_1, Q_2, Q_3, Q_4) \tag{28}$$

$$\begin{aligned} \bar{\delta}(Q_1, Q_2, Q_3, Q_4) &= e_{\zeta}^T(0)Q_1e_{\zeta}(0) + e_1^T(0)Q_2e_1(0) \\ &+ \int_{-\tau(t)}^0 \phi_1^T Q_3 \phi_1 d\alpha + \int_{-\tau(t)}^0 \phi_2^T Q_4 \phi_2 d\alpha \end{aligned} \tag{29}$$

When $t \in [-\tau(t), 0]$, $\hat{\zeta} = 0, \hat{x}_1 = 0, \zeta = \varphi_1(t)$ and $x_1 = \varphi_2(t)$.

Theorem 1 For matrices $C_k > 0$ ($k=1, \dots, 5$) and $Q_{\bar{k}} > 0$ ($\bar{k}=1, \dots, 4$), if matrices P_1, P_2, R_1, R_2 and L_{i3} exist, then $L_{i4}, L_{i5}, \text{prey}\{\Gamma_{i1}, \Gamma_{i2}\}, \mu_1$ and μ_2 ensure that (30) holds:

$$\Pi = \begin{bmatrix} \Pi_1 & \Pi_2 \\ \Pi_2^T & \Pi_3 \end{bmatrix} + \Pi_4^T \Pi_4 < 0 \tag{30}$$

where

$$\Pi_4 = [C_1 \ 0 \ C_2 \ C_3 \ 0 \ 0 \ C_4 \ -C_4 \ C_5] \tag{31}$$

$$\Pi_1 = \begin{bmatrix} \xi_{iw}^{11} & P_1 A_{id0} & \bar{T}_{iw}^T P_2^T & 0 & P_1 L_{i3} \Sigma_2 \\ * & -R_1 & 0 & 0 & 0 \\ * & * & \xi_i^{33} & P_2 A_{id1} & 0 \\ * & * & * & -R_2 & 0 \\ * & * & * & * & -I \end{bmatrix} \tag{32}$$

$$\Pi_2 = \begin{bmatrix} 0 & P_1 N_{i0} & 0 & -P_1 L_{i3} \Sigma_2 D_{i2} \Xi_{i2} \\ 0 & 0 & 0 & 0 \\ P_2 L_{i4} \Sigma_2 & P_2 N_{i1} & \xi_i^{38} & -P_2 L_{i4} \Sigma_2 D_{i2} \Xi_{i2} \\ 0 & 0 & 0 & 0 \\ 0 & 0 & 0 & 0 \end{bmatrix} \tag{33}$$

$$\Pi_3 = \begin{bmatrix} -I & 0 & \Sigma_2^T L_{i5} & 0 \\ * & -\mu_1^2 & 0 & 0 \\ * & * & -2\Gamma_{i1} & L_5 \Sigma_2 D_{i2} \\ * & * & * & -\mu_2^2 \end{bmatrix} \tag{34}$$

$$\xi_{iw}^{11} = (A_{iw0} - L_{i3} \Sigma_2 D_{i0} \Xi_{i0})^T P_1 + P_1 (A_{iw0} - L_{i3} \Sigma_2 D_{i0} \Xi_{i0}) + R_1 + m_1 I \tag{35}$$

$$\xi_i^{33} = (A_{i1} - L_{i4} \Sigma_2 D_{i1} \Xi_{i1})^T P_2 + P_2 (A_{i1} - L_{i4} \Sigma_2 D_{i1} \Xi_{i1}) + R_2 + m_2 I \tag{36}$$

$$\xi_i^{38} = (D_{i1} \Xi_{i1})^T \Sigma_2^T L_{i5}^T - P_2 N_{i1} \tag{37}$$

If the inequalities $P_1 \leq Q_1, P_2 \leq Q_2, R_1 \leq Q_3$ and $R_2 \leq Q_4$ hold, then system (26) is stable and satisfies $J_{\infty} < 0$.

Proof By selecting the positive Lyapunov functions χ_1, χ_2 and χ_3 :

$$\chi_1 = e_{\zeta}^T P_1 e_{\zeta} + \int_0^t [m_1 e_{\zeta}^T(\alpha) e_{\zeta}(\alpha) - h_1^T h_1] d\alpha + \int_{t-\tau(t)}^t e_{\zeta}^T(\alpha) R_1 e_{\zeta}(\alpha) d\alpha \tag{38}$$

$$\chi_2 = e_1^T P_2 e_1 + \int_0^t [m_2 e_1^T(\alpha) e_1(\alpha) - h_2^T h_2] d\alpha + \int_{t-\tau(t)}^t e_1^T(\alpha) R_2 e_1(\alpha) d\alpha \tag{39}$$

$$\chi_3 = \hat{F}_{com}^T \hat{F}_{com} \tag{40}$$

The corresponding derivatives of the functions can be obtained as follows:

$$\begin{aligned} \dot{\chi}_1 &= \Lambda_{(i,w)}(\varpi, \Delta) \{ e_{\zeta}^T [(A_{iw0} - L_{i3} \Sigma_2 D_{i0} \Xi_{i0})^T P_1 + P_1 (A_{iw0} \\ &- L_{i3} \Sigma_2 D_{i0} \Xi_{i0}) + R_1 + m_1 I] e_{\zeta} + 2e_{\zeta}^T P_1 A_{id0} e_{\zeta}(t - \tau(t)) \\ &+ 2e_{\zeta}^T P_1 N_{i0} F_{com} - 2e_{\zeta}^T P_1 L_{i3} \Sigma_2 D_{i2} \Xi_{i2} e_2 + 2e_{\zeta}^T P_1 L_{i3} \Sigma_2 h_1 \\ &- h_1^T h_1 - e_{\zeta}^T(t - \tau(t)) R_1 e_{\zeta}(t - \tau(t)) \} \end{aligned} \tag{41}$$

$$\begin{aligned} \dot{\chi}_2 = & \Lambda_{(i,w)}(\varpi, \Delta)\{e_1^T [(A_{i1} - L_{i4}\Sigma_2 D_{i1} \Xi_{i1})^T P_2 + R_2 + m_2 I \\ & + P_2(A_{i1} - L_{i4}\Sigma_2 D_{i1} \Xi_{i1})]e_1 + 2e_1^T P_2 \bar{T}_{iw} e_\varsigma + 2e_1^T P_2 N_{i1} F_{com} \\ & + 2e_1^T P_2 A_{id1} e_1(t - \tau(t)) - 2e_1^T P_2 L_{i4} \Sigma_2 D_{i2} \Xi_{i2} e_2 - 2e_1^T P_2 N_{i1} \hat{F}_{com} \\ & + 2e_1^T P_2 L_{i4} \Sigma_2 h_2 - h_2^T h_2 - e_1^T (t - \tau(t)) R_2 e_1(t - \tau(t))\} \end{aligned} \tag{42}$$

$$\begin{aligned} \dot{\chi}_3 = & \Lambda_{(i,w)}(\varpi, \Delta)(-2prey\{\Gamma_{i1}\}\hat{F}_{com}^T \hat{F}_{com} + 2e_1^T \Xi_{i1}^T D_{i1}^T \Sigma_2^T L_{i5}^T \hat{F}_{com} \\ & + 2\hat{F}_{com}^T L_{i5} \Sigma_2 D_{i2} \Xi_{i2} e_2 + 2\hat{F}_{com}^T L_{i5} \Sigma_2 h_2) \end{aligned} \tag{43}$$

Define χ as follows:

$$\chi = \chi_1 + \chi_2 + \chi_3 \tag{44}$$

An auxiliary function is set as a second performance indicator, as follows:

$$J_1 = \int_0^t (\|s_\infty\|^2 - \mu_1^2 \|F_{com}(\alpha)\|^2 - \mu_2^2 \|e_2(\alpha)\|^2 + \dot{\chi}(\alpha)) d\alpha \tag{45}$$

The derivation shows that

$$\|s_\infty\|^2 - \mu_1^2 \|F_{com}(t)\|^2 - \mu_2^2 \|e_2(t)\|^2 + \dot{\chi} = q^T \Pi q \tag{46}$$

$$q^T = [e_\varsigma(t) \quad e_\varsigma(t - \tau(t)) \quad F_{com}(t) \quad e_2(t) \quad h_1(t) \quad e_1(t) \quad e_1(t - \tau(t)) \quad \hat{F}_{com}(t)] \tag{47}$$

Π satisfies conditions (30) to (37). Thus, $J_1 < 0$. By deriving from (45) and adjusting the parameters, J_1 is expressed as follows:

$$\begin{aligned} J_1 = & \int_0^t (\|s_\infty\|^2 - \mu_1^2 \|F_{com}(t)\|^2 - \mu_2^2 \|e_2(t)\|^2) dt + \chi(t) - \chi(0) \\ \geq & \|s_\infty\|^2 - \mu_1^2 \|F_{com}(t)\|^2 - \mu_2^2 \|e_2(t)\|^2 - [e_\varsigma^T(0) P_1 e_\varsigma(0) \\ & + e_1^T(0) P_2 e_1(0) + \int_{-\tau(t)}^0 \phi_1^T R_1 \phi_1 d\alpha + \int_{-\tau(t)}^0 \phi_2^T R_2 \phi_2 d\alpha] \end{aligned} \tag{48}$$

When $t \in [-\tau(t), 0]$, condition (49) can be satisfied as follows:

$$[\hat{\zeta} \quad \hat{x}_1 \quad \varsigma \quad x_1] = [0 \quad 0 \quad \varphi_1(t) \quad \varphi_2(t)] \tag{49}$$

The following inequality is obtained on the basis of the previously presented derivation and definition:

$$\begin{aligned} J_\infty < & J_1 + \bar{\delta}(P_1 - Q_1, P_2 - Q_2, R_1 - Q_3, R_2 - Q_4) \\ & \bar{\delta}(P_1 - Q_1, P_2 - Q_2, R_1 - Q_3, R_2 - Q_4) \\ = & [e_\varsigma^T(0) P_1 e_\varsigma(0) + e_1^T(0) P_2 e_1(0) + \int_{-\tau(t)}^0 \phi_1^T R_1 \phi_1 d\alpha \\ & + \int_{-\tau(t)}^0 \phi_2^T R_2 \phi_2 d\alpha] - [e_\varsigma^T(0) Q_1 e_\varsigma(0) + e_1^T(0) Q_2 e_1(0) \\ & + \int_{-\tau(t)}^0 \phi_1^T Q_3 \phi_1 d\alpha + \int_{-\tau(t)}^0 \phi_2^T Q_4 \phi_2 d\alpha] \end{aligned} \tag{50}$$

From (29), we can deduce that $J_1 < 0$:

$$\bar{\delta}(P_1 - Q_1, P_2 - Q_2, R_1 - Q_3, R_2 - Q_4) < 0 \tag{51}$$

Hence, $J_\infty < 0$, the robust stable is proved. The system can mask disturbance and accurately estimate the faults. \square

Adaptive fault tolerance. Given the estimated values, fault-tolerant controller ensures that the PDF tracking errors meet the upper bound and the angles match their ideal values. The expected output PDFs are set as follows:

$$\gamma_g(\rho) = \Phi_g^2(C(\rho)V_g)^2 = (C(\rho)V_g)^2 / (V_g^T \Sigma_1 V_g), \quad \forall \rho \in [a, b] \tag{52}$$

where $\gamma_g(\rho)$ is the expected output PDF and V_g is the weight corresponding to the expected output PDF. Thereafter, let

$$\begin{aligned}
 e_2 &= V - V_g \\
 \Lambda_{(i,w)}(\varpi, \Delta) E_i \Xi_i^{-1} D_i^{-1} \dot{e}_2 &= \Lambda_{(i,w)}(\varpi, \Delta) [E_i \Xi_i^{-1} D_i^{-1} (\dot{V} - \dot{V}_g)] \\
 &= \Lambda_{(i,w)}(\varpi, \Delta) E_i \dot{e}_m
 \end{aligned}
 \tag{53}$$

The tracking error dynamics system is described as follows:

$$\begin{aligned}
 \Lambda_{(i,w)}(\varpi, \Delta) E_i \dot{e}_m &= \Lambda_{(i,w)}(\varpi, \Delta) [A_i e_m + A_{id} e_m(t - \tau(t)) + B_i u(t) \\
 &\quad + N_i F_{com}(t) + B_{id} d(t) + (A_i + A_{id}) x_g]
 \end{aligned}
 \tag{54}$$

where $e_m = x(t) - x_g$. We assume that the system is regular pulseless and $\bar{E}_i = L_{i1} E_i L_{i2} = \begin{bmatrix} I_q & 0 \\ 0 & 0 \end{bmatrix}$ and $L_{i2}^{-1} e_m = \begin{bmatrix} \zeta_1 \\ \zeta_2 \end{bmatrix} = \zeta$, (54) can be rewritten as follows:

$$\begin{aligned}
 \Lambda_{(i,w)}(\varpi, \Delta) \bar{E}_i \dot{\zeta}(t) &= \Lambda_{(i,w)}(\varpi, \Delta) [L_1 A_i L_2 \zeta(t) \\
 &\quad + L_1 A_{id} L_2 \zeta(t - \tau(t)) + L_1 B_i u(t) + L_1 N_i F_{com}(t) \\
 &\quad + L_1 B_{id} d(t) + L_1 (A_i + A_{id}) x_g] \\
 \Lambda_{(i,w)}(\varpi, \Delta) B_i U(t) &= \Lambda_{(i,w)}(\varpi, \Delta) [B_i u(t) + (A_i + A_{id}) x_g] \\
 U(t) &= u(t) + \Lambda_{(i,w)}(\varpi, \Delta) [(B_i^T B_i)^{-1} B_i^T (A_i + A_{id}) x_g]
 \end{aligned}
 \tag{55}$$

For eliminating the disturbance and faults, control inputs are as follows:

$$\begin{aligned}
 U(t) &= \Lambda_{(i,w)}(\varpi, \Delta) [\Gamma_{i3} \int_a^b (\Phi C(\rho) V(t) \\
 &\quad - \Phi_g C(\rho) V_g) d\rho + \text{prey}\{\Gamma_{i4}\} F_{com}(t) + \text{prey}\{\Gamma_{i5}\} d(t)] \\
 &= \Lambda_{(i,w)}(\varpi, \Delta) [\Phi_g \Gamma_{i3} \Sigma_2 D_i \Xi_i P \zeta(t) + \text{prey}\{\Gamma_{i5}\} d(t) \\
 &\quad + \Phi_g \Gamma_{i3} \Sigma_2 V(t) \Phi \lambda_3 (\|V_g\| - \|V(t)\|) + \text{prey}\{\Gamma_{i4}\} F_{com}(t)] \\
 &= \Lambda_{(i,w)}(\varpi, \Delta) [L_{i6} \Sigma_2 D_i \Xi_i P \zeta(t) + L_{i6} \Sigma_2 h_3 \\
 &\quad + \text{prey}\{\Gamma_{i4}\} F_{com}(t) + \text{prey}\{\Gamma_{i5}\} d(t)]
 \end{aligned}
 \tag{56}$$

where $L_{i6} = \Phi_g \Gamma_{i3}$ and $h_3 = \Phi \lambda_3 (\|V_g\| - \|V(t)\|) V(t)$.

Theorem 2 If a positive definite matrix P exists and matrices Γ_{i3} , $\text{prey}\{\Gamma_{i4}\}$ and $\text{prey}\{\Gamma_{i5}\}$ ensure that the LMI in (57) and (58) is valid, then system (54) is stable.

$$\Pi_8 = \begin{bmatrix} \Upsilon_{i4} & A_{id} P^T & B_i L_{i6} \Sigma_2 L_2^{-1} P^T & B_i \Gamma_{i4} / \eta_2 & B_i \Gamma_{i5} / \eta_4 \\ * & -R_1 & 0 & 0 & 0 \\ * & * & -I & 0 & 0 \\ * & * & * & -I & 0 \\ * & * & * & * & -I \end{bmatrix} < 0
 \tag{57}$$

$$\begin{aligned}
 \Upsilon_{i4} &= A_i P^T + P A_i^T + P L_2^{-T} R_1 L_2^{-1} P^T + 2 B_i L_{i6} \Sigma_2 D_i \Xi_i P^T \\
 &\quad + P L_2^{-T} \alpha_3 L_2^{-1} P^T + N_i N_i^T / \eta_1^2 + B_{id} B_{id}^T / \eta_3^2 + \lambda I
 \end{aligned}
 \tag{58}$$

Proof By selecting the following Lyapunov function:

$$v = \Lambda_{(i,w)}(\varpi, \Delta) \zeta^T \bar{E}_i^T \bar{P}^{-T} \zeta + \int_{t-\tau(t)}^t \zeta^T(s) R_1 \zeta(s) ds + \int_0^t \alpha_3 \zeta^T \zeta ds - \int_0^t h_3^T h_3 ds
 \tag{59}$$

Then the derivative of v is obtained as follows:

$$\begin{aligned}
 \dot{v} &= \Lambda_{(i,w)}(\varpi, \Delta) \{ \zeta^T [\bar{P}^{-1} L_1 A_i L_2 + 2 \bar{P}^{-1} \nabla + R_1 + L_2^T A_i^T L_1^T \bar{P}^{-T}] \zeta \\
 &\quad + 2 \zeta^T \bar{P}^{-1} L_1 A_{id} L_2 \zeta(t - \tau(t)) + 2 \zeta^T \bar{P}^{-1} L_1 B_{id} d(t) + 2 \zeta^T (\bar{P}^{-1} L_1 N_i \\
 &\quad + \bar{P}^{-1} L_1 B_i \text{prey}\{\Gamma_{i4}\}) F_{com}(t) + 2 \zeta^T \bar{P}^{-1} L_1 B_i \text{prey}\{\Gamma_{i5}\} d(t) \\
 &\quad - \zeta^T(t - \tau(t)) R_1 \zeta(t - \tau(t)) + 2 \zeta^T \bar{P}^{-1} L_1 B_i L_{i6} \Sigma_2 h_3 + \alpha_3 \zeta^T \zeta - h_3^T h_3 \}
 \end{aligned}
 \tag{60}$$

Inequality (61) can be expressed as follows²⁹:

$$h_3^T h_3 \leq \left(\lambda_3 \|D_i \Xi_i L_2\| / \sqrt{\|\Sigma_1\|} \right)^2 \zeta^T(t) \zeta(t)
 \tag{61}$$

By letting $\alpha_3 = \left(\lambda_3 \|D_i \Xi_i L_2\| / \sqrt{\|\Sigma_1\|} \right)^2$, $\nu \geq 0$ is ensured to be constantly right, hence

$$\begin{aligned}
 \dot{v} \leq & \Lambda_{(i,w)}(\varpi, \Delta) \{ \zeta^T [\bar{P}^{-1} L_1 A_i L_2 + L_2^T A_i^T L_1^T \bar{P}^{-T} + 2\bar{P}^{-1} \nabla + \alpha_3 \\
 & + R_1] \zeta + \eta_4^2 d^T(t) d(t) + 2\zeta^T \bar{P}^{-1} L_1 A_{id} L_2 \zeta(t - \tau(t)) - h_3^T h_3 \\
 & + \eta_3^2 d(t) d(t) + \eta_1^2 F_{com}^T(t) F_{com}(t) - \zeta^T(t - \tau(t)) R_1 \zeta(t - \tau(t)) \\
 & + 2\zeta^T \bar{P}^{-1} L_1 B_i L_{i6} \Sigma_2 h_3 + \eta_2^2 F_{com}^T(t) F_{com}(t) \\
 & + \zeta^T \bar{P}^{-1} L_1 B_i \text{prey}\{\Gamma_{i5}\} (\bar{P}^{-1} L_1 B_i \text{prey}\{\Gamma_{i5}\})^T \zeta \\
 & + \zeta^T \bar{P}^{-1} L_1 N_i (\bar{P}^{-1} L_1 N_i)^T / \eta_1^2 + \zeta^T \bar{P}^{-1} L_1 B_{id} (\bar{P}^{-1} L_1 B_{id})^T \zeta / \eta_3^2 \\
 & + \zeta^T \bar{P}^{-1} L_1 B_i \text{prey}\{\Gamma_{i4}\} (\bar{P}^{-1} L_1 B_i \text{prey}\{\Gamma_{i4}\})^T \zeta / \eta_2^2 \\
 \leq & q^T \Pi_5 q + (\eta_1^2 + \eta_2^2) F_{com}^T(t) F_{com}(t) + (\eta_3^2 + \eta_4^2) d^T(t) d(t)
 \end{aligned} \tag{62}$$

where

$$\nabla = L_1 B_i L_{i6} \Sigma_2 D_i \Xi_i L_2 \tag{63}$$

$$q^T = [\zeta^T \quad \zeta^T(t - \tau(t)) \quad h_3^T] \tag{64}$$

$$\Pi_5 = \Lambda_{(i,w)}(\varpi, \Delta) \begin{bmatrix} \Upsilon_{i1} & \bar{P}^{-1} L_1 A_{id} L_2 & \bar{P}^{-1} L_1 B_i L_{i6} \Sigma_2 \\ * & -R_1 & 0 \\ * & * & -I \end{bmatrix} \tag{65}$$

$$\begin{aligned}
 \Upsilon_{i1} = & \bar{P}^{-1} L_1 A_i L_2 + L_2^T A_i^T L_1^T \bar{P}^{-T} + R_1 + 2\bar{P}^{-1} \nabla + \alpha_3 \\
 & + \bar{P}^{-1} L_1 N_i (\bar{P}^{-1} L_1 N_i)^T / \eta_1^2 + \bar{P}^{-1} L_1 B_{id} (\bar{P}^{-1} L_1 B_{id})^T / \eta_3^2 \\
 & + \bar{P}^{-1} L_1 B_i \text{prey}\{\Gamma_{i4}\} (\bar{P}^{-1} L_1 B_i \text{prey}\{\Gamma_{i4}\})^T / \eta_2^2 \\
 & + \bar{P}^{-1} L_1 B_i \text{prey}\{\Gamma_{i5}\} (\bar{P}^{-1} L_1 B_i \text{prey}\{\Gamma_{i5}\})^T / \eta_4^2
 \end{aligned} \tag{66}$$

By substituting $\bar{P} = L_1 P L_2^{-T}$ and $\bar{P}^{-1} = L_2^T P^{-1} L_1^{-1}$ into Π_5 , the following equations can be derived as

$$\Pi_6 = \Lambda_{(i,w)}(\varpi, \Delta) \begin{bmatrix} \Upsilon_{i2} & L_2^T P^{-1} A_{id} L_2 & L_2^T P^{-1} B_i L_{i6} \Sigma_2 \\ * & -R_1 & 0 \\ * & * & -I \end{bmatrix} \tag{67}$$

$$\begin{aligned}
 \Upsilon_{i2} = & L_2^T P^{-1} A_i L_2 + L_2^T A_i^T P^{-T} L_2 + R_1 + 2L_2^T P^{-1} B_i L_{i6} \Sigma_2 D_i \Xi_i L_2 \\
 & + L_2^T P^{-1} N_i N_i^T P^{-T} L_2 / \eta_1^2 + L_2^T P^{-1} B_{id} B_{id}^T P^{-T} L_2 / \eta_3^2 + \alpha_3 \\
 & + L_2^T P^{-1} B_i \text{prey}\{\Gamma_{i4}\} \Gamma_{i4}^T B_i^T P^{-T} L_2 / \eta_2^2 \\
 & + L_2^T P^{-1} B_i \text{prey}\{\Gamma_{i5}\} \Gamma_{i5}^T B_i^T P^{-T} L_2 / \eta_4^2
 \end{aligned} \tag{68}$$

Π_6 is multiplied by $\text{diag}(P L_2^{-T} \quad I \quad I)$ on the left and $\text{diag}(L_2^{-1} P^T \quad I \quad I)$ on the right. Then first row first column element of Π_6 is added by λI . Hence, (69) is obtained, where λ is a small positive constant.

$$\Pi_7 = \Lambda_{(i,w)}(\varpi, \Delta) \begin{bmatrix} \Upsilon_{i3} & A_{id} P^T & B_i L_{i6} \Sigma_2 L_2^{-1} P^T \\ * & -R_1 & 0 \\ * & * & -I \end{bmatrix} \tag{69}$$

$$\begin{aligned}
 \Upsilon_{i3} = & A_i P^T + P A_i^T + P L_2^{-T} R_1 L_2^{-1} P^T + 2B_i L_{i6} \Sigma_2 D_i \Xi_i P^T + \lambda I \\
 & + P L_2^{-T} \alpha_3 L_2^{-1} P^T + N_i N_i^T / \eta_1^2 + B_{id} B_{id}^T / \eta_3^2 \\
 & + B_i \text{prey}\{\Gamma_{i4}\} \Gamma_{i4}^T B_i^T / \eta_2^2 + B_i \text{prey}\{\Gamma_{i5}\} \Gamma_{i5}^T B_i^T / \eta_4^2
 \end{aligned} \tag{70}$$

When $\Pi_8 < 0$, the following inequality is obtained:

$$\dot{v} \leq -\lambda \zeta^T \zeta + (\eta_1^2 + \eta_2^2) F_{com}^T(t) F_{com}(t) + (\eta_3^2 + \eta_4^2) d^T(t) d(t) \tag{71}$$

We obtain $\Pi_7 < 0$ and $\Pi_8 < 0$, which are equivalent, based on Schur complement theory. Therefore, when $\Pi_8 < 0$ and

$$\|\zeta\|^2 > \frac{M_f^2(\eta_1^2 + \eta_2^2) + M_d^2(\eta_3^2 + \eta_4^2)}{\lambda} \tag{72}$$

$\dot{v} < 0$ is confirmed. Hence, the error system is stable. \square

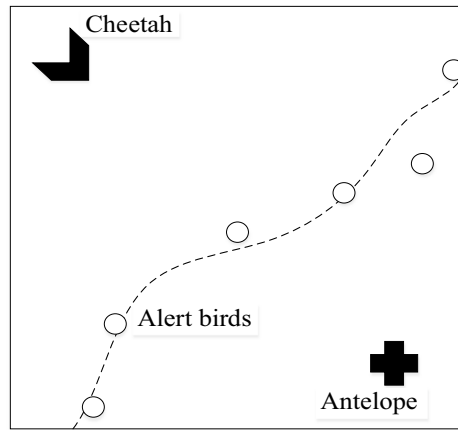


Figure 3. Positional relationship of two animals.

Cheetah		Antelope	
Distance	Status	Judgment	Response
Far	Progressive	Safe	Static
Close	Progressive	Safe	Static
Close	Run	Threat	Run

Table 1. Insensitive prey strategy.

Fault		Controller	
Distance	Status	Judgment	Response
$(0, \kappa]$	Fault free	Incipient impact	$\Gamma_{i11}, \Gamma_{i21}, \Gamma_{i41}, \Gamma_{i51}$
$(\kappa, 0.1\ u(t)\)$	Fault $F_i(t)$	Incipient impact	$\Gamma_{i11}, \Gamma_{i21}, \Gamma_{i41}, \Gamma_{i51}$
$(0.1\ u(t)\ , Mf)$	Fault $F(t)$	Big impact	$\Gamma_{i12}, \Gamma_{i22}, \Gamma_{i42}, \Gamma_{i52}$

Table 2. Insensitive prey algorithm of fault-tolerant control.

In the input (56), the actual value is replaced with the fault estimated value. Thus, the fault-tolerant tracking controller can be expressed as follows:

$$\begin{aligned}
 u(t) &= \Lambda_{(i,w)}(\varpi, \Delta)[U(t) - (B_i^T B_i)^{-1} B_i^T (A_i + A_{id})x_g] \\
 &= \Lambda_{(i,w)}(\varpi, \Delta)[L_{i6} \Sigma_2 D_i \Xi_i P \zeta(t) - (B_i^T B_i)^{-1} B_i^T (A_i + A_{id})x_g \\
 &\quad + \text{prey}\{\Gamma_{i5}\} \hat{d}(t) + \text{prey}\{\Gamma_{i4}\} \hat{F}_{com}(t) + L_{i6} \Sigma_2 h_3]
 \end{aligned}
 \tag{73}$$

Bionic parameter varying architecture. A bionic strategy that mimics animal predation allows parameters set to be optimal for incipient actuator faults, enhancing the tracking performance. An antelope can use the surrounding birds to judge threat from cheetah and respond to it by running or continue grazing². Figure 3 shows the position.

Prey strategy originates from the cheetah/antelope hunting process. Accordingly, we replace cheetah and antelope with fault and controller, respectively. Tables 1 and 2 provides the corresponding relationship of insensitive prey strategy, where $\Gamma_{i11}, \Gamma_{i21}, \Gamma_{i41}, \Gamma_{i51}, \Gamma_{i12}, \Gamma_{i22}, \Gamma_{i42}, \Gamma_{i52}$ are the LMI-compliant adaptive learning rates, $\kappa \in R^+$ is approximately zero.

Remark 3 The boundary state cheetah (progressive, close) corresponds to the boundary state interval $(\kappa, 0.1\|u(t)\|)$ in which $u(t)$ determines the fault magnitude in Tables 1 and 2, $\kappa \ll 0.1\|u(t)\|$. The insensitive prey controller determines that the faults in the interval have minimal effect, thereby retaining the learning rates. The sensitive prey controller is the opposite.

Figure 4 is a decision tree showing the architecture of the prey algorithm. The algorithm steps are as follows: *Step 1* Fault amplitude is less than or equal to κ , no fault, parameters are set to $\Gamma_{i11}/\Gamma_{i21}/\Gamma_{i41}/\Gamma_{i51}$.

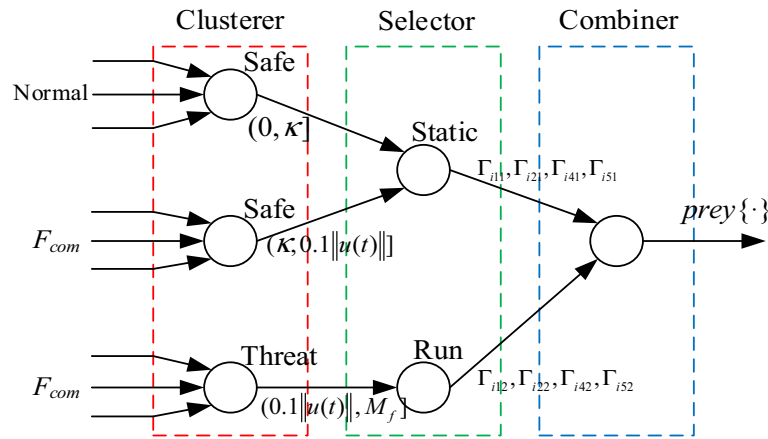


Figure 4. Strategic architecture.

Step 2 Fault amplitude is larger than κ and less than or equal to $0.1\|u(t)\|$, incipient fault, parameters are insensitive and set to $\Gamma_{i11}/\Gamma_{i21}/\Gamma_{i41}/\Gamma_{i51}$.

Step 3 Fault amplitude is larger than $0.1\|u(t)\|$, large value fault, parameters are set to $\Gamma_{i12}/\Gamma_{i22}/\Gamma_{i42}/\Gamma_{i52}$.

Step 4 Return to Step 1 without modifying content.

On the basis of Table 1 and 2, and Fig. 2, (22) and (73) can be improved to prey adaptive estimation and fault-tolerant controller as follows:

$$\begin{cases} \dot{\hat{F}}_{com}(t) = \Lambda_{(i,w)}(\varpi, \Delta)(-prey\{\Gamma_{i1}\}\hat{F}_{com}(t) + prey\{\Gamma_{i2}\}\varepsilon(t)) \\ u(t) = \Lambda_{(i,w)}(\varpi, \Delta)[L_{i6}\Sigma_2 D_i \Xi_i P \zeta(t) + L_{i6}\Sigma_2 h_3 + prey\{\Gamma_{i5}\}\hat{d}(t) \\ \quad + prey\{\Gamma_{i4}\}\hat{F}_{com}(t) - (B_i^T B_i)^{-1} B_i^T (A_i + A_{id})x_g] \end{cases} \quad (74)$$

where $prey\{\Gamma_{i1}, \Gamma_{i2}, \Gamma_{i4}, \Gamma_{i5}\}$ are the hybrid learning rates designed according to the prey strategy satisfied:

$$prey\{\Gamma_{i1}, \Gamma_{i2}\} = \begin{cases} \Gamma_{i11}, \Gamma_{i21}, & \|\hat{F}_{com}(t)\| \in (0, \kappa] \text{ or } (\kappa, 0.1\|u(t)\|] \\ \Gamma_{i12}, \Gamma_{i22}, & \|\hat{F}_{com}(t)\| \in (0.1\|u(t)\|, M_f] \end{cases} \quad (75)$$

$$prey\{\Gamma_{i4}, \Gamma_{i5}\} = \begin{cases} \Gamma_{i41}, \Gamma_{i51}, & \|\hat{F}_{com}(t)\| \in (0, \kappa] \text{ or } (\kappa, 0.1\|u(t)\|] \\ \Gamma_{i42}, \Gamma_{i52}, & \|\hat{F}_{com}(t)\| \in (0.1\|u(t)\|, M_f] \end{cases} \quad (76)$$

Remark 4 Prey algorithm makes estimation and fault-tolerant control processes more sensitive to the incipient deviation, hence HFV has the ability to predict and repair early signs. We define a set of faults with incipient deviation element and other deviation element to indicate that the controller can handle the individual occurrence of all fault deviation elements ($F_1(t)$ and $F(t)$).

Simulation experiment

HFV model. The validity should be verified via a semi-physical simulation. The PDFs of HFV that describes the attitude angle uncertainty are approximated by the weights and B-spline similar to that in (7) as follows:

$$\varphi_{11}(\rho) = \varphi_{22}(\rho) = \varphi_{33}(\rho) = 0.8(\rho - 4)^2 I_3 + (-\rho^2 + 5\rho - 23.5)I_4 + 0.8(\rho - 7)^2 I_5 \quad (77)$$

$$\varphi_{12}(\rho) = \varphi_{23}(\rho) = \varphi_{31}(\rho) = 0.3(\rho - 3)^2 I_2 + (-\rho^2 + 8\rho - 19.5)I_3 + 0.8(\rho - 6)^2 I_4 \quad (78)$$

$$\varphi_{13}(\rho) = \varphi_{21}(\rho) = \varphi_{32}(\rho) = 0.7(\rho - 2)^2 I_1 + (-\rho^2 + 10\rho - 11.5)I_2 + 0.1(\rho - 5)^2 I_3 \quad (79)$$

where $I_{\bar{i}}(\bar{i} = 1, \dots, 5)$ are interval functions defined as follows:

$$I_{\bar{i}} = \begin{cases} 1, & \rho \in [\bar{i} + 1, \bar{i} + 2] \\ 0, & \text{otherwise} \end{cases}$$

Based on system (1) and the characteristics of the three outputs in HFV, the basis function matrix has three vectors generating three attitude angle PDFs. Both the reference ρ_{in} and the outputs ρ_{out} in Fig. 1 can be converted into corresponding PDFs.

In the fuzzy HFV dynamics, the prerequisite variable is assumed to be w_3 , which is an element of the weight vector $V(t)$. In the fuzzy disturbance dynamics, the prerequisite variable is assumed to be d_1 , which is an element of the rudder interference $d(t)$. The membership functions are expressed as follows:

$$\begin{cases} h_1(\varpi) = 1/[1 + \exp(-1.73w_3)] \\ h_2(\varpi) = 1 - h_1 \end{cases} \tag{80}$$

$$\begin{cases} h_1(\Delta) = 1/[1 + \exp(6 + 28d_3)] \\ h_2(\Delta) = 1 - h_1(\Delta) \end{cases} \tag{81}$$

Two rules of double-fuzzy approximation systems:

Rule 1: IF w_3 is approximately 0.8, THEN: $\{E_1 A_1 A_1 d H_1 B_1 D_1 \Xi_1 B_1 d\}$,

Rule 2: IF w_3 is approximately 0.1, THEN: $\{E_2 A_2 A_2 d H_2 B_2 D_2 \Xi_2 B_2 d\}$.

Rule 1: IF d_1 is approximately 0.04, THEN: $\{T_1 \Omega_1\}$,

Rule 2: IF d_1 is approximately 0.12, THEN: $\{T_2 \Omega_2\}$.

The inertia ($t \times m^2$) in (5) and (6) is expressed as follows: $J = \begin{bmatrix} 55.486 & 0 & -23.002 \\ 0 & 1136.949 & 0 \\ -23.002 & 0 & 1376.852 \end{bmatrix}$.

The system state matrices can be calculated by setting the linearised roller speed and system (1). Hence, the parameter matrices in systems (10) and (11) are expressed as follows:

$$\begin{aligned} E_1 = E_2 &= \begin{bmatrix} 1 & 1 & 0 \\ 0 & 1 & 0 \\ 0 & 0 & 0 \end{bmatrix}, \quad \Xi_1 = \Xi_2 = \begin{bmatrix} 0.99 & 0 & 0.06 \\ 0.06 & 3 & -0.99 \\ 0 & 1 & 0 \end{bmatrix}, \quad A_1 = \begin{bmatrix} 0.05 & 3.02 & -2.5 \\ -0.01 & 0 & 0.25 \\ 0 & -0.11 & 0.05 \end{bmatrix}, \quad A_2 = \begin{bmatrix} 0.06 & 2.98 & -3.75 \\ -0.01 & 0 & 0.37 \\ 0.01 & -0.19 & 0.06 \end{bmatrix}, \\ A_{1d} &= \begin{bmatrix} -0.1 & -0.5 & 0.12 \\ 0.2 & -0.25 & 0.06 \\ 0 & 0 & 0.6 \end{bmatrix}, \quad A_{2d} = \begin{bmatrix} -0.1 & -0.3 & -0.1 \\ 0 & -0.05 & -0.1 \\ 0 & 0 & -0.9 \end{bmatrix}, \quad B_1 = \begin{bmatrix} 1 & 1 & -0.01 \\ 0 & 2 & -0.02 \\ 0.002 & 0.005 & 0.1 \end{bmatrix}, \quad B_2 = \begin{bmatrix} 0.9 & 0.9 & -0.01 \\ 0 & 2 & -0.02 \\ 0.001 & 0.001 & 0.1 \end{bmatrix}, \\ D_1 &= \begin{bmatrix} 1 & 0 & 0 \\ 0 & 1 & 0 \\ 0 & 0 & 1 \end{bmatrix}, \quad D_2 = \begin{bmatrix} 2 & 0 & 0 \\ 0 & 3 & 0 \\ 0 & 0 & 5 \end{bmatrix}, \quad H_1 = \begin{bmatrix} 0.1 \\ 0.3 \\ 0.3 \end{bmatrix}^T, \quad H_2 = \begin{bmatrix} 0.1 \\ 0.2 \\ 0.2 \end{bmatrix}^T, \quad B_{1d} = B_{2d} = \begin{bmatrix} 0.1 & 0.1 & -0.01 \\ 0 & 0.2 & -0.02 \\ 0.002 & 0.005 & 0.1 \end{bmatrix}. \end{aligned}$$

H_1 and H_2 are the equivalent matrices of N_1 and N_2 . Delay time: $\tau(t) = 0.5(\sin t + 1)$, the parameter matrices of $d(t)$:

$$T_1 = \begin{bmatrix} 2 & 0 & 0 \\ 0 & 0 & 0 \\ 0 & 0 & 0 \end{bmatrix}, \quad T_2 = \begin{bmatrix} 1 & 0 & 0 \\ 0 & 0 & 0 \\ 0 & 0 & 0 \end{bmatrix}, \quad \Omega_1 = \begin{bmatrix} 0 & 4 & 0 \\ -4 & 1 & 0 \\ 0 & 0 & 2 \end{bmatrix}, \quad \Omega_2 = \begin{bmatrix} 0 & 8 & 0 \\ -3 & 0 & 0 \\ 0 & 0 & 1 \end{bmatrix}.$$

The expected weight matrix is set as $V_g = [0.7 \ 0.7 \ 0.79]^T$. According to the incipient fault $F_1(t)$ defined by inequality (3) and the relationship between states and weights, we set the incipient and standard deviation faults as follows:

$$F_1(t) = \begin{cases} 0, & t < 5s \\ 0.07, & t \geq 5s \end{cases} \tag{82}$$

$$F(t) = \begin{cases} 0, & t < 5s \\ 0.25, & t \geq 5s \end{cases} \tag{83}$$

Reference input parameters are taken as $C_4 = C_5 = 0.1$, $C_1 = [0.1 \ 0.1 \ 0.1 \ 0.1 \ 0.1]$, $C_2 = C_3 = [0.2 \ 0.2]$. This section solves the LMI in Theorems 1 and 2 for: $L_{i3} - L_{i5}$, $\Gamma_{i1} - \Gamma_{i5}$, prey learning rates Γ_{i11} , Γ_{i21} , Γ_{i41} , Γ_{i51} , Γ_{i12} , Γ_{i22} , Γ_{i42} , and Γ_{i52} are obtained through repeated experiments. Thereafter, the matrices are substituted into the stochastic HFV.

Platform and results. We use the Links-Box semi-physical simulator to verify the effectiveness of the algorithms. Links-Box automatically converts the MATLAB simulation model of HFV to the embedded control prototype and support engineering hardware to test in the model. Then HFV physical device defined in the hardware environment can dynamically verify the controller performance. The features of software package Links-RT are:

1. Adapt to the HFV model built in MATLAB;
2. Provide input/output hardware to enable users to integrate the hardware environment into HFV model;
3. Automatic conversion of MATLAB model codes to VxWorks codes;
4. Provide communication, storage, scheduling and other services in VxWorks.



Figure 5. Semi-physical simulation platform.

Error	$F_1(t)$			$F(t)$		
	ρ_1	ρ_2	ρ_3	ρ_1	ρ_2	ρ_3
TM (e_{ss1})/rad	Me: 0.04	0.04	0.04	0.22	0.22	0.22
	Mi: 0.013	0.012	0.014	0.219	0.218	0.219
	Ma: 0.07	0.07	0.07	0.221	0.221	0.222
NM (e_{ss1})/rad	Me: 0	0.0001	0.0001	0.0001	0.0002	0.0001
	Mi: 0	0	0	0	0	0
	Ma: 0.0001	0.0002	0.0001	0.0001	0.0003	0.0002
TM (e_{ss2})/deg	Me: 0.09	0.08	0.08	0.07	0.06	0.07
	Mi: 0	0	0	0	0	0
	Ma: 0.14	0.12	0.13	0.11	0.1	0.11
NM (e_{ss2})/deg	Me: 0.012	0.011	0.01	0.01	0.008	0.008
	Mi: 0	0	0	0	0	0
	Ma: 0.02	0.017	0.016	0.014	0.011	0.011

Table 3. Comparison between TM and NM.

The simulation platform is shown in Fig. 5.

Table 3 compares the results of the traditional method (TM) of HFV in¹¹ and our new method (NM). e_{ss1} and e_{ss2} are the steady-state error absolute values of estimation and tolerance. Me, Mi and Ma are the mean, minimum and maximum, respectively. Table 3 shows that the method in¹¹ is insufficiently effective for the HFV with non-Gaussian stochastic attitudes. The NM is more stable and accurate than TM.

Augmented observer (16) shows the ideal and estimation results of disturbance in Fig. 6. The function vector is as follows:

$$d(t) = [0.07 \sin(t + 0.32) \ 0 \ 0]^T \tag{82}$$

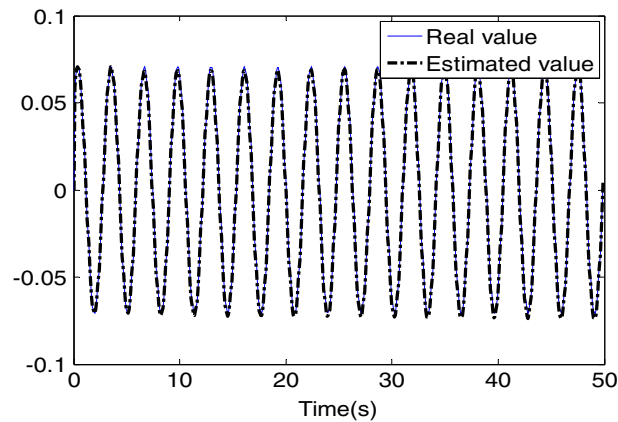


Figure 6. Disturbance curve and its estimation.

The estimation results of disturbance are substituted into system (22), whilst the effective results of fault estimation are shown in Fig. 7. The estimation curves of the three attitude angles (ρ_1 , ρ_2 , and ρ_3) are slightly different. However, the incipient and total faults are well estimated.

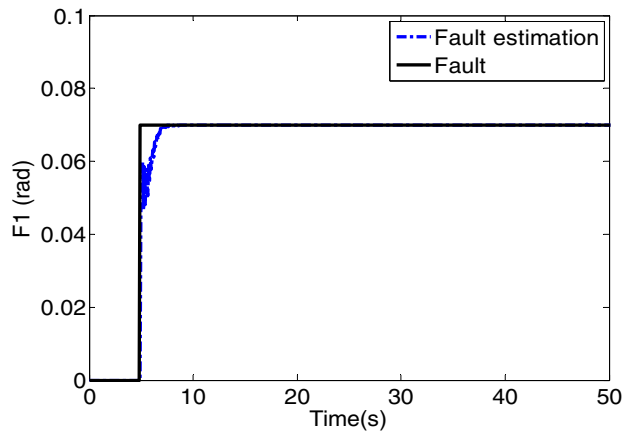
Figure 8 shows the PDF plots of the stochastic attitude angle outputs under the prey adaptive tolerant controller (64). Fault-tolerant results show that prey adaptive controller can accurately track the ideal PDFs.

Experiment shows that for incipient faults and large deviation faults, the controller can limit the tracking errors and response times of the attitude PDFs in an acceptable ranges. Table 3 shows the PDF tracking errors in Fig. 8. The response time range is: 2–3.5 s. Based on Fig. 8, Table 4 statistics the performance and mean data of the PDFs. The mean values can be calculated by online simulation through formula (8).

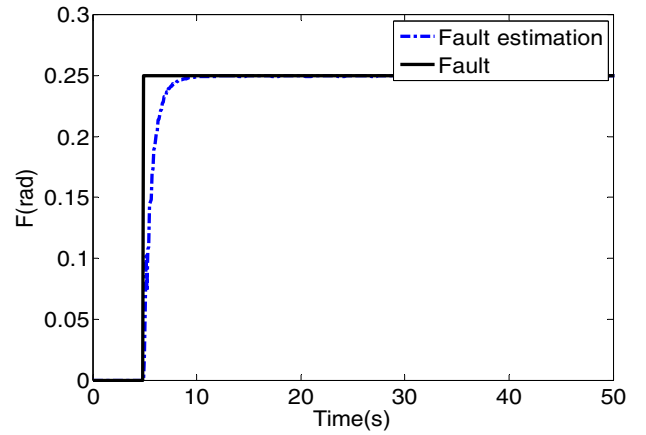
In Table 4, t_{res} is the response time and e_{max} is the maximum steady-state error in the cross section. Angle unit: deg, and time unit: second. The tracking response time of an attitude mean is shorter than that of PDF, because the stabilization of the PDF shape needs more shape indicators to be stable at the same time, which takes longer, but can make the control better. The FTC algorithm has a good attitude tracking effect and can meet the engineering requirements of HFV.

Conclusion

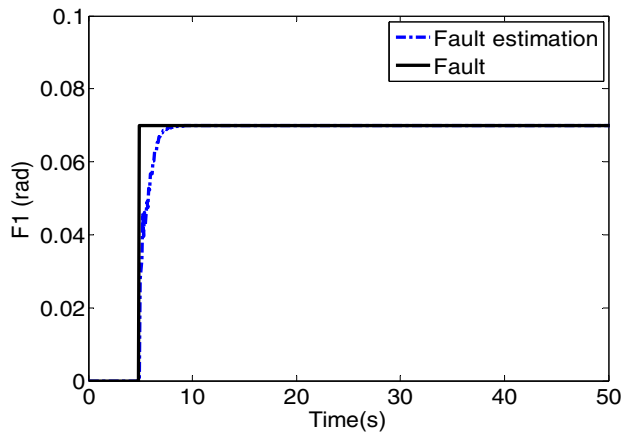
AN HFV model with attitude angle non-Gaussian uncertainty is proposed. This model uses PDFs to show more attitude angle information than the definitive mean and variance. HFV fault information and self-healing are determined through a change in the PDF shapes, thereby improving the fault self-healing and anti-laser capability. In double-fuzzy approximation linearized dynamics, the DOB effectively estimates the disturbance. Then a fault estimation observer is designed with the estimated disturbance to minimise the defined performance index. The strategy mimics the animal predation process successfully used to design controllers. Bionic prey adaptive FTC compensates for the effects of faults with different amplitudes on the three angle PDFs. The controller with no fault estimation has part of the direct repair function, thence estimation can help complete the repair without full fault amplitudes, the tolerance time is shorter than the estimation time. The output and ideal PDFs are consistent, good performance is verified in the simulation. This method constructs the control technology system of random aircraft, creates the condition for the design and implementation of anti-laser weapon, and has the frontier and application value.



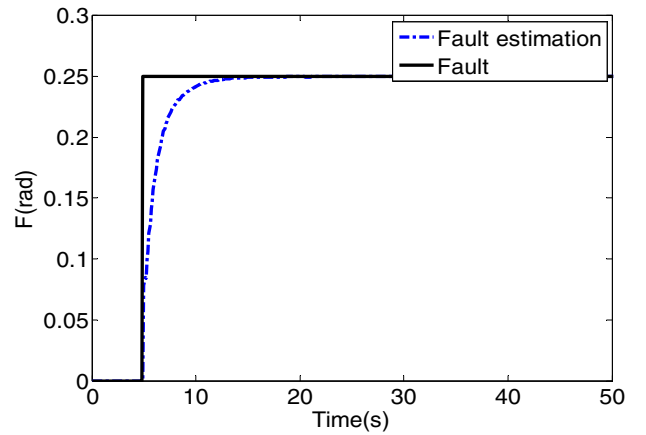
(a) Incipient deviation (ρ_1)



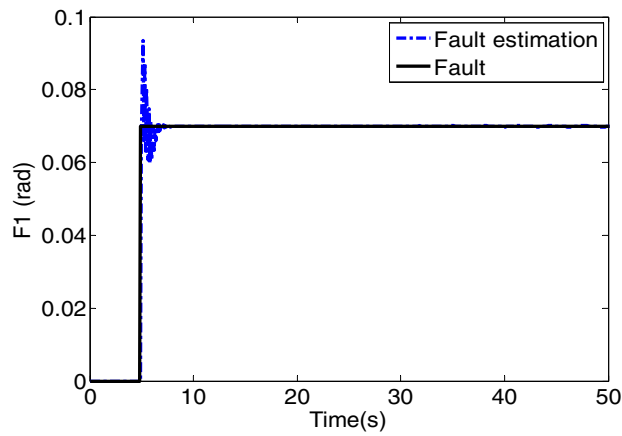
(b) Superimposed deviation (ρ_1)



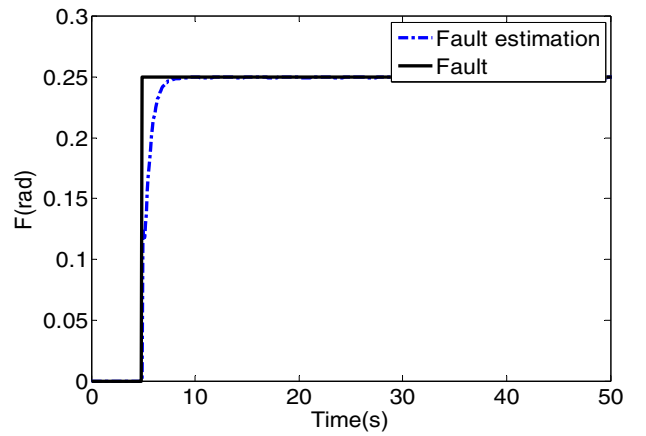
(c) Incipient deviation (ρ_2)



(d) Superimposed deviation (ρ_2)



(e) Incipient deviation (ρ_3)



(f) Superimposed deviation (ρ_3)

Figure 7. Fault estimation.

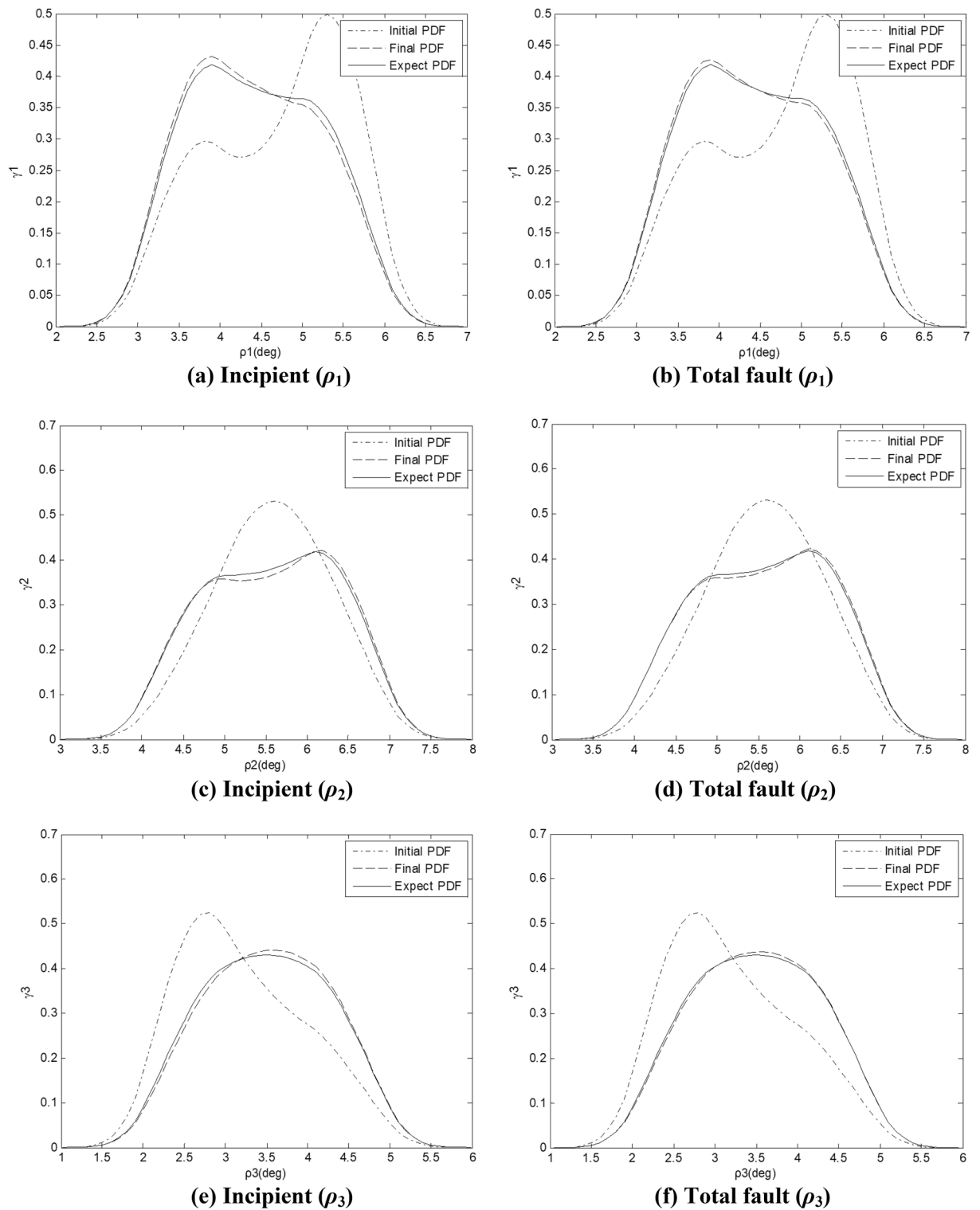


Figure 8. Expected and final PDFs.

Performance	ρ_1	ρ_2	ρ_3
Mean(F_1/F)	4.383/4.388	5.774/5.768	3.682/3.685
$t_{res}(F_1/F)$	1.491/2.232	1.416/2.208	1.028/1.995
$e_{max}(F_1/F)$	0.014/0.019	0.011/0.017	0.011/0.014

Table 4. Fault tolerance tracking performance.

Received: 3 August 2022; Accepted: 10 November 2022

Published online: 15 November 2022

References

- Hu, K. Y., Chen, F. Y. & Cheng, Z. A. Fuzzy adaptive hybrid compensation for compound faults of hypersonic flight vehicle. *Int. J. Control Autom. Syst.* **19**, 2269–2283. <https://doi.org/10.1007/s12555-019-0474-x> (2021).
- Wang, L., Qi, R. R. & Jiang, B. Adaptive actuator fault-tolerant control for non-minimum phase air-breathing hypersonic vehicle model. *ISA Trans.* **126**, 47–64. <https://doi.org/10.1016/j.isatra.2021.07.032> (2022).
- Shao, X. D., Hu, Q. L., Shi, Y. & Jiang, B. Y. Fault-tolerant prescribed performance attitude tracking control for spacecraft under input saturation. *IEEE Trans. Control Syst. Technol.* **28**, 574–582. <https://doi.org/10.1109/TCST.2018.2875426> (2020).
- Zhao, D., Jiang, B. & Yang, H. Backstepping-based decentralized fault-tolerant control of hypersonic vehicles in PDE-ODE form. *IEEE Trans. Autom. Control* **67**, 1210–1225. <https://doi.org/10.1109/TAC.2021.3059689> (2022).
- Hu, Q. L., Shao, X. D. & Guo, L. Adaptive fault-tolerant attitude tracking control of spacecraft with prescribed performance. *IEEE/ASME Trans. Mechatron.* **23**, 331–341. <https://doi.org/10.1109/TMECH.2017.2775626> (2018).
- Cui, L. & Yang, Y. Disturbance rejection and robust least-squares control allocation in flight control system. *J. Guid. Control Dyn.* **34**, 1632–1643. <https://doi.org/10.2514/1.52234> (2011).
- An, H., Liu, J. X., Wang, C. H. & Wu, L. G. Disturbance observer-based antiwindup control for air-breathing hypersonic vehicles. *IEEE Trans. Ind. Electron.* **63**, 3038–3049. <https://doi.org/10.1109/TIE.2016.2516498> (2016).
- Yu, M. Y., Feng, Z. G., Huang, J. J. & Yu, Y. T. Characteristic extraction of rolling bearing compound faults of aero-engine. *J. Vibroeng.* **19**, 4285–4299. <https://doi.org/10.21595/jve.2017.18612> (2017).
- Huang, M. Q., Tian, M. & Zhou, J. Parameter optimization of PID controller for water and fertilizer control system based on partial attraction adaptive firefly algorithm. *Sci. Rep.* **12**, 12182. <https://doi.org/10.1038/s41598-022-16425-7> (2022).
- Yuan, Y., Wang, Z., Guo, L. & Liu, H. P. Barrier Lyapunov functions-based adaptive fault tolerant control for flexible hypersonic flight vehicles with full state constraints. *IEEE Trans. Syst. Man Cybern. Syst.* **50**, 3391–3400. <https://doi.org/10.1109/TSMC.2018.2837378> (2020).
- Shen, Q. K., Jiang, B. & Cocquemot, V. Fault-tolerant control for T-S fuzzy systems with application to near-space hypersonic vehicle with actuator faults. *IEEE Trans. Fuzzy Syst.* **20**, 652–665. <https://doi.org/10.1109/TFUZZ.2011.2181181> (2012).
- He, J. J., Qi, R. Y. & Jiang, B. Fault-tolerant control with mixed aerodynamic surfaces and RCS jets for hypersonic reentry vehicles. *Chin. J. Aeronaut.* **30**, 780–795. <https://doi.org/10.1016/j.cja.2017.01.003> (2017).
- Hu, Q. L., Wang, C. L., Li, Y. & Huang, J. Adaptive control for hypersonic vehicles with time-varying faults. *IEEE Trans. Aerosp. Electron. Syst.* **54**, 1442–1455. <https://doi.org/10.1109/TAES.2018.2793319> (2018).
- Jiang, B., Gao, Z. F., Shi, P. & Xu, Y. F. Adaptive fault-tolerant tracking control of near-space vehicle using Takagi-Sugeno fuzzy models. *IEEE Trans. Fuzzy Syst.* **18**, 1000–1007. <https://doi.org/10.1109/TFUZZ.2010.2058808> (2010).
- Kaushal, H. & Kaddoum, G. Applications of lasers for tactical military operations. *IEEE Access* **5**, 20736–20753. <https://doi.org/10.1109/ACCESS.2017.2755678> (2017).
- Cai, J. H., Chen, S. P. & Hou, J. 1.1-kW peak-power dissipative soliton resonance in a mode-locked Yb-fiber laser. *IEEE Photonics Technol. Lett.* **29**, 2191–2194. <https://doi.org/10.1109/LPT.2017.2768487> (2017).
- Yao, L. N., Qin, J. F., Wang, H. & Jiang, B. Design of new fault diagnose and fault tolerant control scheme for non-Gaussian singular stochastic distribution systems. *Automatica* **48**, 2305–2313. <https://doi.org/10.1016/j.automatica.2012.06.036> (2012).
- Sun, Y. C. & Liang, Z. H. Fault diagnosis and fault tolerant control for non-Gaussian singular time-delayed stochastic distribution systems with disturbance based on the rational square-root model. *J. Control Sci. Eng.* **4**, 1–12. <https://doi.org/10.1155/2016/9563481> (2016).
- Wang, L. X. A new look at Type-2 fuzzy sets and Type-2 fuzzy logic systems. *IEEE Trans. Fuzzy Syst.* **25**, 693–706. <https://doi.org/10.1109/TFUZZ.2016.2543746> (2017).
- Mohammad, M. E. & Armin, S. B. IC-FNN: a novel fuzzy neural network with interpretable, intuitive, and correlated-contours fuzzy rules for function approximation. *IEEE Trans. Fuzzy Syst.* **26**, 1288–1302. <https://doi.org/10.1109/TFUZZ.2017.2718497> (2018).
- Yao, L. N. & Lei, C. H. Fault diagnosis and sliding mode fault tolerant control for Non-Gaussian stochastic distribution control systems using T-S fuzzy model. *Asian J. Control* **19**, 636–646. <https://doi.org/10.1504/IJMIC.2018.089626> (2017).
- Dong, J. X. & Yang, G. H. Observer-based output feedback control for discrete-time T-S fuzzy systems with partly immeasurable premise variables. *IEEE Trans. Syst. Man Cybern. Syst.* **47**, 98–110. <https://doi.org/10.1109/TSMC.2016.2531655> (2017).
- Feng, Y. & Yagoubi, M. On state feedback H_∞ control for discrete-time singular systems. *IEEE Trans. Autom. Control* **58**, 2674–2679. <https://doi.org/10.1109/TAC.2013.2256051> (2013).
- Kwon, N. K., Park, I. S., Park, P. & Park, C. Dynamic output-feedback control for singular Markovian jump system: LMI approach. *IEEE Trans. Autom. Control* **62**, 5396–5400. <https://doi.org/10.1109/TAC.2017.2691311> (2017).
- Yao, L. N. & Feng, L. Fault diagnosis and fault tolerant tracking control for the non-Gaussian singular time-delayed stochastic distribution system with PDF approximation error. *Neurocomputing* **175**, 538–543. <https://doi.org/10.1016/j.neucom.2015.10.092> (2016).
- Cui, P. L., Zhang, D. H., Yang, S. & Li, H. T. Friction compensation based on time-delay control and internal model control for a gimbal system in magnetically suspended CMG. *IEEE Trans. Ind. Electron.* **64**, 3798–3807. <https://doi.org/10.1109/TIE.2016.2644620> (2017).
- Roy, S., Kar, I. N., Lee, J. & Jin, M. L. Adaptive-robust time-delay control for a class of uncertain Euler–Lagrange systems. *IEEE Trans. Ind. Electron.* **64**, 7109–7119. <https://doi.org/10.1109/TIE.2017.2688959> (2017).
- Hu, K. Y., Li, W. H. & Cheng, Z. A. Fuzzy adaptive fault diagnosis and compensation for variable structure hypersonic vehicle with multiple faults. *PLoS ONE* **16**, e0256200. <https://doi.org/10.1371/journal.pone.0256200> (2021).
- Wang, H., Kang, Y. F., Yao, L. N., Wang, H. & Gao, Z. W. Fault diagnosis and fault tolerant control for T-S fuzzy stochastic distribution systems subject to sensor and actuator faults. *IEEE Trans. Fuzzy Syst.* **29**, 3561–3569. <https://doi.org/10.1109/TFUZZ.2020.3024659> (2021).
- Chen, H. T., Jiang, B. & Lu, N. Y. Deep PCA based real-time incipient fault detection and diagnosis methodology for electrical drive in High-Speed Trains. *IEEE Trans. Veh. Technol.* **67**, 4819–4830. <https://doi.org/10.1109/TVT.2018.2818538> (2018).

Acknowledgements

The project was supported by the National Natural Science Foundation of China under Grant 61773201. This research was also supported by the 173 key project of the Chinese Military Science and Technology Commission.

Author contributions

K.-Y.H. and W.S. conceived the research, performed the research and wrote the manuscript. K.Z. performed the research, revised the manuscript and provided the fund support.

Competing interests

The authors declare no competing interests.

Additional information

Correspondence and requests for materials should be addressed to K.-Y.H.

Reprints and permissions information is available at www.nature.com/reprints.

Publisher's note Springer Nature remains neutral with regard to jurisdictional claims in published maps and institutional affiliations.



Open Access This article is licensed under a Creative Commons Attribution 4.0 International License, which permits use, sharing, adaptation, distribution and reproduction in any medium or format, as long as you give appropriate credit to the original author(s) and the source, provide a link to the Creative Commons licence, and indicate if changes were made. The images or other third party material in this article are included in the article's Creative Commons licence, unless indicated otherwise in a credit line to the material. If material is not included in the article's Creative Commons licence and your intended use is not permitted by statutory regulation or exceeds the permitted use, you will need to obtain permission directly from the copyright holder. To view a copy of this licence, visit <http://creativecommons.org/licenses/by/4.0/>.

© The Author(s) 2022